Dynamic cross-frequency couplings of local field potential oscillations in rat striatum and hippocampus during performance of a T-maze task

Adriano B. L. Tort[a,b,1], Mark A. Kramer[a], Catherine Thorn[c,d], Daniel J. Gibson[c,e], Yasuo Kubota[c,e], Ann M. Graybiel[c,e,2], and Nancy J. Kopell[a,1,2]

[a]Department of Mathematics and Center for BioDynamics, Boston University, Boston, MA 02215; [b]Department of Biochemistry, Federal University of Rio Grande do Sul, Porto Alegre, RS 90035, Brazil; and [c]McGovern Institute for Brain Research and Departments of [d]Electrical Engineering and Computer Science, and [e]Brain and Cognitive Sciences, Massachusetts Institute of Technology, Cambridge, MA 02139

Contributed by Nancy J. Kopell, October 21, 2008 (sent for review August 19, 2008)

Oscillatory rhythms in different frequency ranges mark different behavioral states and are thought to provide distinct temporal windows that coherently bind cooperating neuronal assemblies. However, the rhythms in different bands can also interact with each other, suggesting the possibility of higher-order representations of brain states by such rhythmic activity. To explore this possibility, we analyzed local field potential oscillations recorded simultaneously from the striatum and the hippocampus. As rats performed a task requiring active navigation and decision making, the amplitudes of multiple high-frequency oscillations were dynamically modulated in task-dependent patterns by the phase of cooccurring theta-band oscillations both within and across these structures, particularly during decision-making behavioral epochs. Moreover, the modulation patterns uncovered distinctions among both high- and low-frequency subbands. Cross-frequency coupling of multiple neuronal rhythms could be a general mechanism used by the brain to perform network-level dynamical computations underlying voluntary behavior.

amplitude modulation | gamma | theta

Oscillations in neural population voltage activity are universal phenomena (1). Among brain rhythms, theta oscillations in local field potentials (LFPs) recorded in the hippocampus are prominent during active behaviors (2–5), and these have long been intensively analyzed in the rodent in relation to spatial navigation (6), memory (7), and sleep (8). Theta-band rhythms (4–12 Hz) are now known to occur in other cortical (9–12) and subcortical (12–15) regions, however, including the striatum (14–17), studied here. Gamma oscillations (30–100 Hz) have also received special attention because of their proposed role in functions such as sensory binding (18), selective attention (19–21), transient neuronal assembly formation (22), and information transmission and storage (23–25). The existence of physiologically meaningful neocortical oscillations at even higher frequencies, above the traditional gamma range, has been reported as well (10, 26–28). In rodents, for example, brief sharp-wave associated ripples (120–200 Hz) appear in the hippocampal formation during slow wave sleep, immobility and consummatory behavior, characteristically in the absence of theta waves (2, 29).

The oscillatory activities conventionally assigned to different frequency bands are not completely independent (2–4, 9, 10, 30). In one type of interaction, the phase of low-frequency rhythms modulates the amplitude of higher-frequency oscillations (9, 10, 30). For example, theta phase is known to modulate gamma power in rodent hippocampal and cortical circuits (2–4, 31), and the phase of theta rhythms recorded in the human neocortex can modulate wide-band (60–200 Hz) high-frequency oscillations (10). Such theta–gamma nesting is thought to play a role in sequential memory organization and maintenance of working memory, and more generally in "phase coding" (25, 31). Based on evidence suggesting that theta rhythms in hippocampal and striatal memory circuits are coordinated in rats during learning and performance of a conditional T-maze task (14), we asked whether theta phase modulates cooccurring high-frequency oscillations in the striatum as well as in the hippocampus, and if so whether such cross-frequency effects occur between the 2 structures, and whether the phase–amplitude coupling is related to specific behavioral performance. We demonstrate here that distinct bands of high-frequency oscillations are modulated by ongoing low-frequency rhythms, both within and across the striatum and hippocampus. We further show that the strength of these cross-frequency interactions changes dynamically, and differentially, during different epochs of behavioral performance requiring decision and action. These findings suggest that the cross-frequency interactions reflect behaviorally relevant simultaneous activation of synchronized striatal and hippocampal memory circuits.

Results

We analyzed the LFP oscillatory activity recorded in the dorsal caudoputamen and the CA1 field of the dorsal hippocampus as rats ($n = 6$) navigated a T-maze in which they turned right or left in response to auditory instruction cues indicating which of the 2 end arms was baited with chocolate (14, 15) (Fig. 1*A*). In both the striatum and the hippocampus, theta power increased as the rats left the start zone, peaked as the animals traversed the maze, and diminished as the rats approached the goal [Figs. 1 *B* and *C* and 2 *A* and *B* and supporting information (SI) Fig. S1]. By contrast, low gamma power (LG, 30–60 Hz) diminished during the middle of the task, and high gamma (HG, 60–100 Hz) and high-frequency oscillations (HFO, >100 Hz) powers increased throughout the maze runs (Figs. 1 *B* and *C* and 2 *A* and *B* and Fig. S1). Notably, these modulations in power had different time courses in the 2 structures (see Figs. 1 *B* and *C* and 2 *A* and *B* and Fig. S1).

To determine whether interactions across these frequency ranges occurred, we developed a cross-frequency measure to analyze phase-to-amplitude modulation in limited-time datasets (modulation index, see *SI Text*). This method allowed us to examine phase–amplitude modulation for successive event epochs during the maze runs. Phase-to-amplitude comodulograms were constructed by applying this measure to multiple frequency band pairs made up of "phase frequency" and "amplitude frequency" bands stepped through task time (Figs. 1*D* and 2 *C* and *D* and Fig. S2).

Author contributions: A.M.G. and N.J.K. designed research; A.B.L.T., C.T., D.J.G., and Y.K. performed research; A.B.L.T., M.A.K., C.T., D.J.G., Y.K., A.M.G., and N.J.K. analyzed data; and A.B.L.T., M.A.K., A.M.G., and N.J.K. wrote the paper.

The authors declare no conflict of interest.

[1]To whom correspondence may be addressed. E-mail: tort@bu.edu or nk@bu.edu.

[2]A.M.G. and N.J.K. contributed equally to this work.

This article contains supporting information online at www.pnas.org/cgi/content/full/0810524105/DCSupplemental.

NEUROSCIENCE

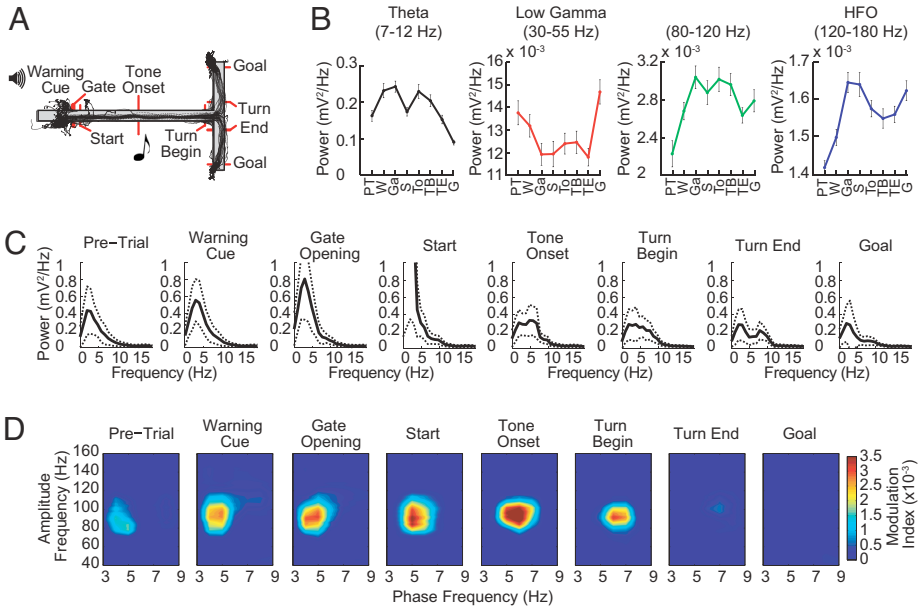

Fig. 1. Dynamic amplitude modulation of fast LFP rhythms by theta phase in the striatum during maze runs. (*A*) T-maze with task events and run trajectories from a representative session with 39 trials. Red markers show photobeam positions. (*B*) Average power of striatal oscillations for successive event windows (1 s) over 4 frequency ranges of interest. Error bars represent SEM. Event labels: PT, pre-trial; W, warning cue; Ga, gate opening; S, start; To, tone onset; TB, turn begin; TE, turn end; G, goal reaching. (*C*) Mean power spectra (solid lines) showing characteristic changes in the power peak during perievent windows. Dashed lines represent ±SD. (*D*) Phase-to-amplitude comodulograms plotted for each task-event window. Pseudocolor scale represents modulation index values shown at right. Positive values indicate a statistically significant ($P < 0.01$) phase-to-amplitude cross-frequency coupling (see *SI Text*). Results illustrated in *B–D* were obtained from a striatal tetrode in a representative rat by analyzing all trials in the session shown in *A*.

In both the striatum and the hippocampus, phase–amplitude couplings characteristically emerged as the animals traversed the maze and tended to disappear at goal reaching (Figs. 1*D* and 2 *C* and *D*). In the striatum, theta-band oscillations dynamically modulated a narrow band of higher-frequency oscillations (≈80–120 Hz), and the modulation tended to occur at low (≈3–8 Hz) theta frequencies (Fig. 1*D*). Theta phase in the hippocampus modulated the amplitude of a wider range of high frequencies (≈40–350 Hz), with the strongest coupling occurring at the HFO frequency band (Figs. 2*C* and 4*D* and Fig. S3). The theta-band oscillations responsible for phase–amplitude coupling in the hippocampus were in a narrower band and generally higher in frequency (≈8–12 Hz) than those in the striatum (Figs. 1*D* and 2 *C* and *D*, but see Fig. S4). Phase-to-amplitude modulation in the hippocampus was found in all 6 rats studied; modulation in the striatum was found in 4 of the 6 rats studied.

Within both structures, the couplings exhibited consistent patterns. In the striatum, 80- to 120-Hz oscillations peaked at the troughs of the theta wave (Fig. 3), a pattern similar to that reported for electrocorticogram recordings of oscillatory activity in the human neocortex (10). In the hippocampus, phase–amplitude interactions depended on both the frequency band

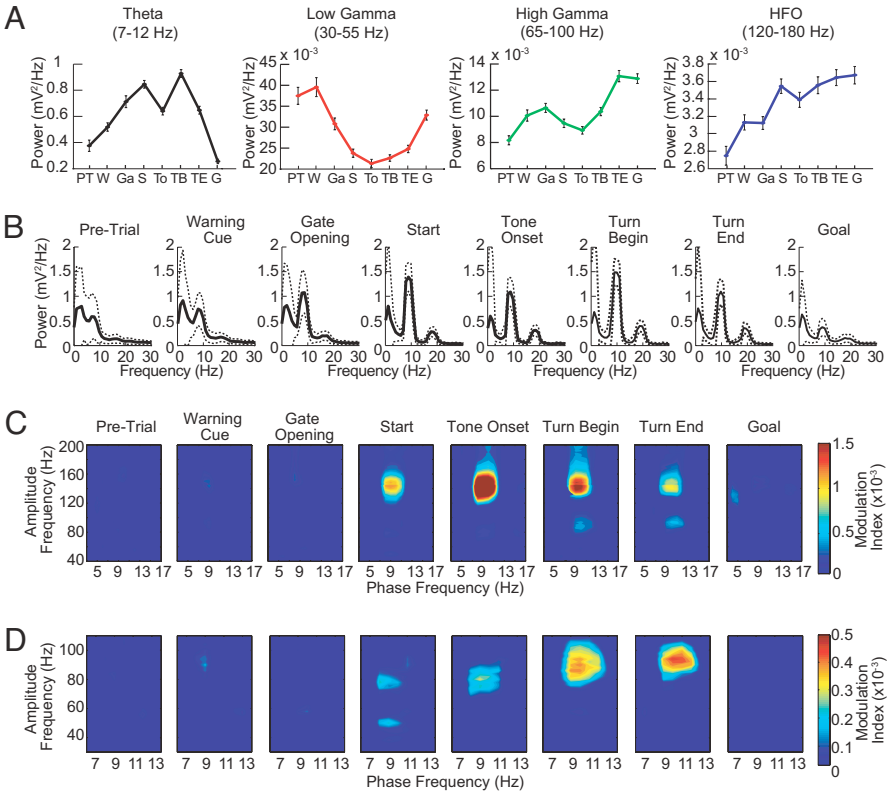

Fig. 2. Phase-to-amplitude modulation in the hippocampus. (*A*) Average power of hippocampal oscillations recorded in CA1 and plotted for each task-event window over 4 frequency ranges of interest. Events are labeled as in Fig. 1*B*. (*B*). Mean power spectra recorded during the successive task epochs. (*C* and *D*) Phase-to-amplitude comodulograms obtained from LFPs recorded during the distinct task-event windows shown. Plots in *C* show amplitude modulation of rhythms over the entire high-frequency range studied (40–200 Hz). Plots in *D* show modulation in the high frequency range focused on gamma, from 30 to 110 Hz. Results illustrated in *A–D* were obtained from a tetrode in the superficial layer of CA1 in a representative rat by analyzing all trials ($n = 40$) in a session.

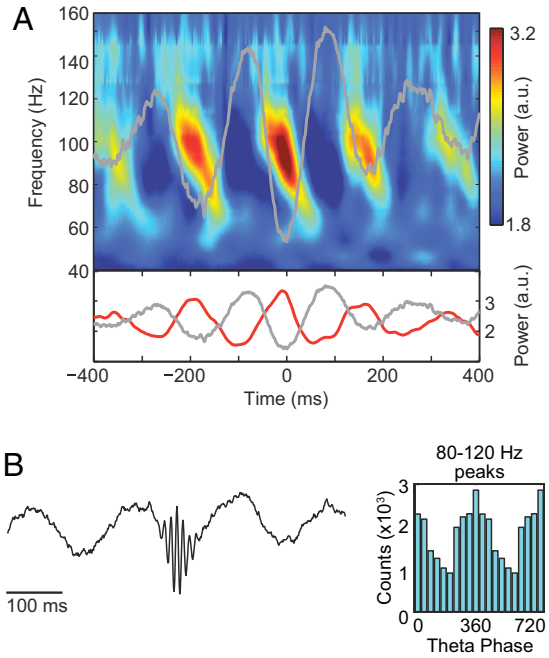

Fig. 3. The amplitude of striatal 80–120 Hz LFP oscillations is maximal at the troughs of cooccurring striatal theta oscillations. (*A*) (*Upper*) Time–frequency plot of the mean normalized power time-locked to the theta (5–8 Hz) trough. (*Lower*) Plot showing the mean normalized power at 100 Hz (red line). The theta trough-locked averaged raw signal is shown in both *Upper* and *Lower* plots as a gray line. (*B*) (*Left*) Averaged raw signal obtained by aligning the LFP traces at the peaks of the 80- to 120-Hz oscillation (see *SI Text*). (*Right*) The histogram of the theta phases at which the peaks occurred. Results were obtained from the same animal and experimental session as in Fig. 1.

and the CA1 layer in which the recordings were made. The HG and HFO amplitudes peaked at the trough of the theta oscillation at the deep recording sites (Fig. 4 *A–C Left* and Fig. S5). At the superficial recording sites, the HG power peaked on the rising phase of theta, and the HFO power was maximal near the peak of the theta wave (Fig. 4 *A–C Right* and Fig. S5). The opposite preferred theta phase for the HFO powers recorded at the deep and superficial layers* likely relates to the well-established phase-reversal of the theta rhythm across the CA1 layers also evident in our recordings (Fig. S5; see also ref. 3). However, this reversal does not account for the differences in preferred phases between the HFO and HG frequency bands in the superficial CA1 layers.

The amplitude modulation of high-frequency rhythms by cooccurring theta was correlated with the power of theta both in the striatum and in the hippocampus, with stronger modulation occurring at greater theta powers (Figs. S6 and S7). The strongest comodulations thus occurred during the middle parts of the maze runs. However, the presence of the theta rhythm per se did not guarantee the existence of the cross-frequency phase-to-amplitude coupling. The peak of theta power in the striatal LFPs did not always match the peak of the cross-frequency modulation observed in the striatum (e.g., Fig. 1 *C* and *D*). In the hippocampal LFPs, clear theta peaks occurred during the pre-trial, warning cue, gate-opening, and goal-reaching periods, when cross-frequency coupling was typically not observed (see Fig. 2 *B–D*). Moreover, comparable levels of hippocampal theta were associated with different modulation index values (e.g., compare the "Gate Opening" and "Tone Onset" events in Fig. 2).

*Roughly, "superficial" and "deep" CA1 layers correspond to stratum pyramidale and stratum lacunosum-moleculare, respectively; see *SI Text*.

Multiple regression analysis demonstrated that for any given high-frequency rhythm, the amplitude modulation depended partly on its own power and partly on the power of other high-frequency rhythms, in addition to the power of the cooccurring theta rhythm (Fig. S7). Likewise, although the animals' running speeds increased up to the middle of the maze runs and then decreased toward goal reaching, the relation between the intensity of the cross-frequency coupling and the animals' speed was not a straightforward one: Speed-controlled analyses demonstrated that changes in speed alone cannot account for the distinct levels of modulation among the task events (Fig. S8).

The presence of phase-amplitude coupling during the midrun period suggested that the coupling might be related to the presence of heightened coherence between the striatal and the hippocampal rhythms, which also tends to occur during this epoch (14). As shown in Fig. 5 for the "Tone Onset" period, cross-structure coupling did occur. The phase–amplitude couplings between the striatal theta phase and the amplitude of the hippocampal fast oscillations were very prominent (Fig. 5*A*, third image from the left). The hippocampal theta modulation of striatal 80- to 120-Hz oscillations was much weaker (Fig. 5*A*, second image from the left). Notably, the striatal–hippocampal cross-structure coupling was strongest at the high theta-band frequencies (8–12 Hz), frequencies that within the hippocampus modulated hippocampal gamma and HFO rhythms, and frequencies at which the striatal and hippocampal theta rhythms were most highly coherent (Fig. 5*C*, see also ref. 14). By contrast, it was the low-frequency striatal theta band (3–8 Hz) that modulated the striatal 80- to 120-Hz oscillations, frequencies at which the striatal and hippocampal theta rhythms were less coherent (Fig. 5*C*). The cross-structure coupling patterns were thus consistent with the patterns of coherence between the theta rhythms in the striatum and hippocampus. Cross-structure phase–amplitude interactions could therefore occur, but they were constrained by subbands within the traditional theta range. It is striking that the frequency constraints for intrastriatal phase–amplitude coupling are different from the constraints for striatal–hippocampal coupling.

A relation between behavioral learning and patterns of striatal–hippocampal theta coherence has been suggested because high levels of cross-structure theta coherence were found in rats that learned the T-maze task used here but not in rats that failed to learn the task (14). In our analysis, we found clear examples of correlations between the phase-amplitude modulation and learning scores (Fig. S9). Our dataset was inappropriate to analyze fully the relationship between the modulation index and the percentage correct performance of all of the rats (see Fig. S9 legend). However, this initial analysis suggests that the phase–amplitude coupling we detected may be related to learning state as well as to active on-line behavioral state.

Discussion

Our findings were unequivocal in suggesting that phase–amplitude coupling is a prominent feature of the oscillatory LFP activity both in the striatum and in the hippocampus under conditions of active, goal-oriented behavior. These dynamic phase–amplitude modulations were distinct for different high-frequency bands modulated by theta phase and for different subbands within the theta range and thus suggested previously undescribed, behaviorally relevant frequency ranges for both striatal and hippocampal oscillations. Moreover, the phase of striatal theta could modulate high-frequency oscillations not only in the striatum but also in the hippocampus, and hippocampal–striatal modulation also was present. Adjustments in phase–amplitude coupling thus occurred not only within but also across striatal and hippocampal circuits during active behavior. The strongest phase–amplitude coupling tended to occur during behavioral epochs involving decision and behavioral choice, suggesting that the couplings relate, at least in part, to ongoing cognitive demands. These findings suggest that dynamic, frequency-

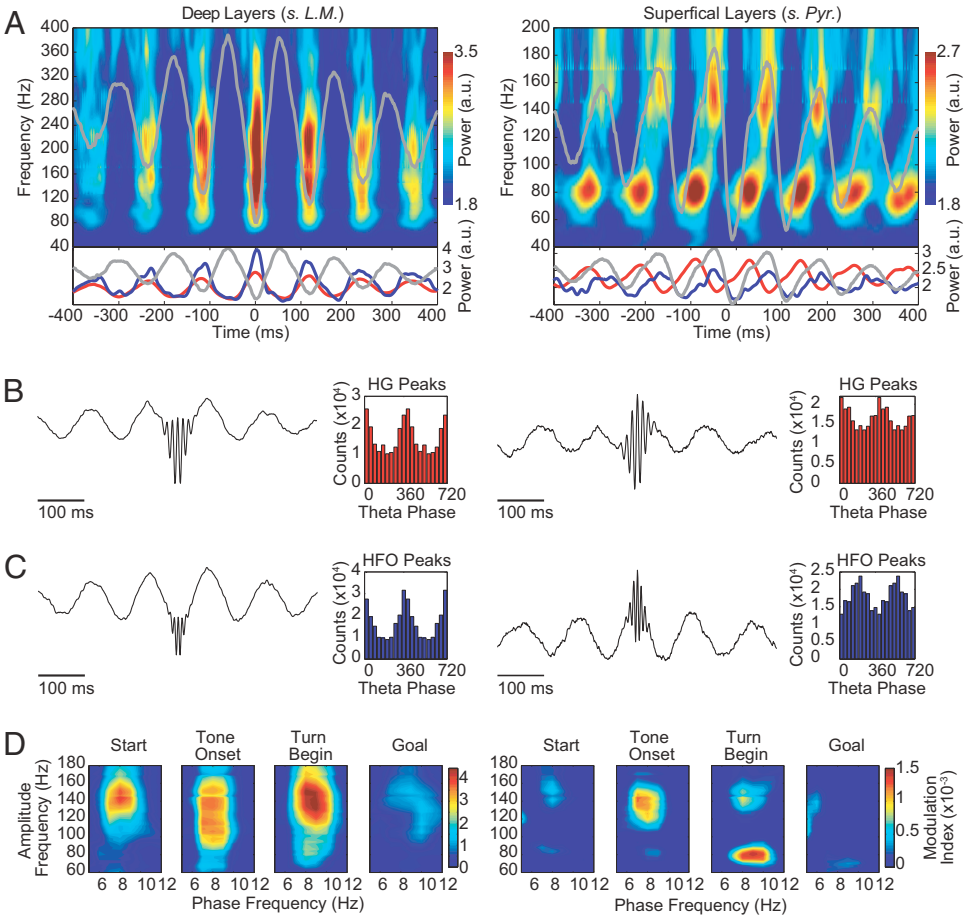

Fig. 4. The theta phase modulation of high-frequency hippocampal LFP oscillations differs for rhythms in different frequency bands and layers in the CA1 region of the dorsal hippocampus. (*A*) (*Upper*) Time–frequency plots of the mean normalized power time-locked to the theta (7–12 Hz) trough for the deep (*Left*) and superficial (*Right*) CA1 layers recordings. (*Lower*) Plots showing the mean normalized power at 80 Hz (HG, red line) and at 160 Hz (HFO, blue line). The theta trough-locked averaged raw signal is shown in gray in all plots. (*B* and *C*) Averaged raw signal obtained by centering the LFP traces at the peaks of the HG (*B*) or HFO (*C*) and the corresponding histograms of the theta phases at which the peaks occurred. (*D*) Phase-to-amplitude comodulograms showing differential theta modulations of HG and HFO rhythms. Results are shown for simultaneous recordings from 1 deep (left column) and 1 superficial (right column) CA1 layer tetrode in a representative rat.

specific phase–amplitude coupling may be a key feature coordinating the activity of striatal and hippocampal learning circuits during sequential voluntary behavior.

Multiple High-Frequency Bands Are Modulated by Theta Phase. The striatal high-frequency range for which we found amplitude modulation by striatal theta phase was ≈80–120 Hz. It is striking that we did not observe phase–amplitude coupling for the low-gamma (30–60 Hz) range, which is the main gamma band so far analyzed in LFP recording experiments in the rodent striatum (14–17, 32, 33). Furthermore, the theta frequencies for which we found the modulation tended to be in the low theta range (≈3–8 Hz), despite the cooccurrence of strong theta oscillations at higher frequencies within the theta band (≈8–12 Hz). Oscillatory activity in the striatal LFPs likely reflect rhythms in striatal inputs both from distant sources such as the thalamus and neocortex and from local sources, particularly the pallidum, itself part of a subthalamo–pallidal oscillatory circuit (34, 35). Interneurons in the striatum have also been found to exhibit oscillatory activity, and although some of their oscillatory activity has been linked to that of the neocortex, some

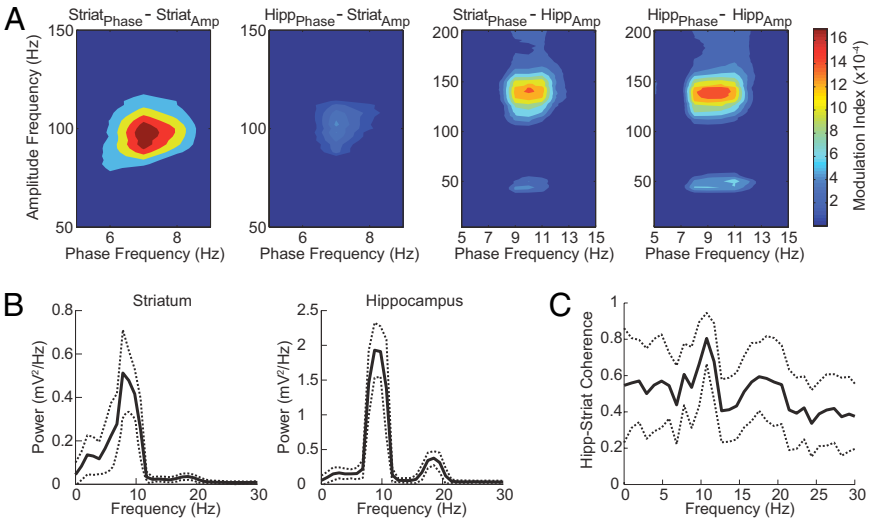

Fig. 5. Phase-amplitude couplings occur between simultaneously recorded striatal and hippocampal oscillations. (*A*) Phase-to-amplitude comodulograms obtained during a 1-s interval around the Tone Onset task event. Results are shown for all phase–amplitude combinations as labeled. Note that the theta phase in each structure modulates the amplitude of oscillations in the other structure. (*B*) Mean power spectrum (solid line) of the LFPs recorded in each brain region during the same task period (Tone Onset), showing a peak in the theta band in both regions. Dashed lines represent ±SD. (*C*) Coherence spectrum (solid line) between the striatal and the hippocampal oscillations during the same task period showing a peak of coherence at ≈10 Hz. Results were obtained from a representative animal during a session (different rat than in Fig. 1).

may be intrinsic or be driven by intrastriatal networks (16, 36, 37). For most of these potential sources, the presence of phase–amplitude coupling has not been examined. However, our finding that the modulated high-frequency striatal LFP oscillations tend to occur at the trough of striatal theta, in the pattern of neocortical theta–gamma modulations, suggests that the striatal couplings are part of a broader network of oscillatory activity coupling that includes the neocortex. Cross-frequency coupling between 8 and 12 Hz and gamma oscillations has been reported for the human nucleus accumbens (38). Moreover, the phases of maximal gamma amplitude were reported to vary between trials in which subjects won or lost. These findings suggest a relationship to reward circuits and, thus, like our own findings, point to a potential function for cross-frequency coupling effects in basal ganglia-based circuits.

In contrast to this striatal phase–amplitude coupling, theta–gamma modulation in the hippocampus is well-known. Hippocampal theta modulates 30- to 100-Hz frequencies as rats engage in exploratory behavior (3). In addition, high-frequency ripples (140–200 Hz) are modulated by lower-frequency sharp-wave events during periods of rest and sleep (2, 29). Here, we demonstrate simultaneous modulation of both traditional gamma-frequency oscillations (30–100 Hz) and higher-frequency rhythms (>100 Hz) by ongoing hippocampal theta as rats perform a T-maze task. Our results suggest that within the traditional gamma frequency interval (2–4, 9, 10, 23–28), there are 3 distinct bands for hippocampal LFP oscillations modulated by theta rhythms: LG, HG, and HFO.

The LG and HG hippocampal oscillations varied differently in power during different parts of the maze runs and also had different phase–amplitude modulation patterns. Overall, theta phase tended to modulate HG activity more than LG activity in the CA1 region (see Fig. S3). The LG and HG activity thus may represent independent physiological processes, a conclusion in accord with findings for gamma rhythms recorded in the olfactory bulb (39). The HG and HFO oscillations were also distinct. Their theta modulations were strongest at different times during the maze runs (Figs. 2 *C* and *D*, 4*D Right*, and Fig. S8*C*), were modulated to different degrees by theta phase (Figs. 2 *C* and *D*, 4*D*, and Fig. S8*C*), peaked at different phases of theta (Fig. 4 *A–C Right*), and were mutually independent (Fig. S7*b*). These findings may relate to the proposal that, in the human neocortex, "low gamma" (30–60 Hz) and "high gamma" (≈60–250 Hz but typically focused on 80–150 Hz) can be distinguished (27) and may result from independent physiological mechanisms with different functions (26–28). Given the heterogeneity in nomenclature, we reserve the term "gamma" to denote the lower high-frequency ranges that have been characterized as inhibition-based (40).

The HFO that we identified in the phase–amplitude analyses probably are distinct from the hippocampal ripple oscillations, because the latter are usually accompanied by sharp waves and are not related to the theta rhythm (2, 29, 31). They are also likely not the hippocampal "very fast oscillations" (VFO) described as depending on axonal gap junctions (41), because these have been most prominently observed in the stratum oriens of the CA1 region and were shown to be modulated by the gamma rhythm (42), in contrast to the HFO described here. One possibility is that the HFO are the remnants of the spiking activity detected by the tetrodes. Another possibility is that the HFO result from entorhinal synaptic input to CA1 (43) and HG from CA3 input. If so, cross-frequency analyses could be used to study entorhinal and CA3 influences on CA1 activity and their functions in relation to memory and navigation.

Cross-Coupling of Low- and High-Frequency Oscillations Occurs Across Striatal and Hippocampal Circuits. In addition to prominent within-structure phase–amplitude coupling in the striatum and hippocampus, we found cross-structure coupling. This coupling was particularly evident for striatal theta phase modulation of hippocampal fast oscillations. The relative weakness of hippocampal–striatal phase–amplitude coupling that we detected raises the possibility that these coupling interactions are asymmetric. Like the within-structure phase–amplitude modulation, the cross-structure modulation was strongest during midrun, the period in which coherence between the theta rhythms in the striatum and hippocampus is maximal (14). The cross-structure couplings were highly frequency-dependent, however, suggesting that they represent specific coupling of striatal–hippocampal rhythms rather than simply a general synchronization of the LFP activity in these 2 structures. The striatum and hippocampus have largely been considered as parallel, and even competing, learning and memory systems engaged differentially in procedural and episodic memory function (44–47). Our findings raise the possibility that these 2 circuitries can interact at multiple levels, including not only by coherence within their theta bands (14), but also by modulation of their high-frequency oscillations by low-frequency oscillations in the other structure.

The existence of such dynamic cross-coupling presents a challenge to the view that activity in single frequency bands satisfactorily captures the oscillatory activity related to particular brain states. Considered together with previous observations (3, 4, 9, 10, 31, 48), our findings suggest, instead, that multiple coexisting patterns of cross-frequency coupling occur and may actually better characterize different states. Our observation of cross-structure striatal–hippocampal coupling is a striking demonstration of this possibility. We observed prominent phase–amplitude coupling for intrastriatal rhythms at low theta-band striatal LFP frequencies (≈3–8 Hz), and cooccurring striatal–hippocampal phase–amplitude coupling for higher-frequency (≈8–12 Hz) striatal LFP oscillations. This finding highlights the possibility that simultaneously activated oscillations, even within a single "band" such as theta, may characterize different behavioral and cognitive states.

It has been proposed that "phase coded" information is used in the hippocampus for representing locations in space and items held in working memory (25). Cross-frequency coupling such as we report here may also serve as a form of phase coding, in which, in addition to single spikes relative to phase, bursts of oscillatory activity would gate or convey information for neural computation.

Cross-Coupling Is Strongest During Decision-Making Epoch. Within the hippocampus, phase–amplitude modulation peaked during the decision period of the task, but was weak before locomotion onset and during the approach to goal. This timing could not be accounted for solely by running speed. This pattern raises the possibility that the modulation of gamma-band activity and HFO in the hippocampus occurs especially when the rat is actively accessing sequential information during locomotion or navigation, but is weak or absent during other periods of the task, despite the presence of prominent theta activity. In the striatum, phase–amplitude modulation also was strongest during the tone-turn decision period and, again, could not be accounted for by running speed. We also found that the modulation could be high early in the trial (periods of low velocity) and that it could be low during turning (high-velocity periods). This large spread of the modulation across the different events within the runs suggests that phase–amplitude modulation in the striatum could be related to the active recall or throughput of sequential information related to task performance. Notably, the tone-turn period is the period in which the lowest density of spiking by striatal projection neurons occurs in rats that have acquired the task (49). The cross-coupled oscillatory patterns could thus especially reflect the accessing of inputs by striatal circuitry. Interestingly, in the one rat in which fully adequate records were available at all sessions, there was a clear learning-related increase in the phase–amplitude coupling both within the striatum and within the hippocampus.

The finding that cross-couplings were most prominent as the rats neared the choice point of the maze raises the possibility that cognitive processes related to decision, choice, and selection influ-

enced the appearance of the phase–amplitude couplings both within the striatum and the hippocampus and across these forebrain regions. If so, this decision phase may be one that particularly calls for multiple frequency-band coordination of striatal and hippocampal activity. This behavioral epoch also appears to be the time at which network coherence within the theta band is enhanced across hippocampal, prefrontal, and striatal circuits (14, 50). These findings suggest that phase–amplitude coupling may reflect the engagement across different time scales of network activity related to active cognitive processing.

Materials and Methods

Behavioral training and electrophysiology recording methods were approved by the Committee on Animal Care of Massachusetts Institute of Technology and are described in detail in refs. 14 and 15. Briefly, 6 male Sprague–Dawley rats were implanted with head stages containing 12 tetrodes, with 6 tetrodes targeting the dorsomedial caudoputamen (AP: +1.7 mm, ML: 1.8 mm, DV: 3.6–4.6 mm) and 6 tetrodes targeting the dorsal CA1 region of the hippocampus (AP: −3.3 mm, ML: 2.2 mm, DV: 2.4–2.8 mm). Tetrodes were lowered to their target depths during a 1-week postsurgical recovery period. Rats then received daily training sessions (usually 40 trials) on an auditory tone-cued T-maze task. Rats were trained to turn right or left at the choice point of the maze as instructed by 1- and 8-kHz tone cues. A click warning cue preceded the opening of a start gate. Rats were rewarded with chocolate sprinkles if the baited goal was correctly approached. Throughout training, LFPs were amplified (gain: 1,000), filtered (1–475 Hz) and continuously sampled at 1 kHz by using a Cheetah recording system (Neuralynx). In the hippocampus, the definition of ''deep'' and ''superficial'' CA1 layers of the dorsal hippocampus was performed based on the phase reversal of the theta wave combined with daily records of tetrode depth. All analyses were done with MATLAB 7.5 software (MathWorks). Details are given in *SI Text*.

ACKNOWLEDGMENTS. We thank Miles Whittington and Roger Traub for comments on a preliminary version of this manuscript. This work was supported by Coordenação de Aperfeiçoamento de Pessoal de Nível Superior (CAPES), Brazil (A.B.L.T.), the Burroughs Wellcome Fund (A.B.L.T., M.A.K., and N.J.K.), a National Science Foundation Research Training Grant (to A.B.L.T., M.A.K., and N.J.K.), a Friends of the McGovern Institute for Brain Research Graduate Student Fellowship (to C.T.), National Institutes of Health Grant MH60379 (to C.T., D.J.G., Y.K., and A.M.G.), and Office of Naval Research Grant N00014-04-1-0208 (to C.T., D.J.G., Y.K., and A.M.G.).

1. Buzsaki G (2006) *Rhythms of the Brain* (Oxford Univ Press, Oxford).
2. Buzsaki G, *et al.* (2003) Hippocampal network patterns of activity in the mouse. *Neuroscience* 116:201–211.
3. Bragin A, *et al.* (1995) Gamma (40–100 Hz) oscillation in the hippocampus of the behaving rat. *J Neurosci* 15:47–60.
4. Hentschke H, Perkins MG, Pearce RA, Banks MI (2007) Muscarinic blockade weakens interaction of gamma with theta rhythms in mouse hippocampus. *Eur J Neurosci* 26:1642–1656.
5. Kahana MJ, Sekuler R, Caplan JB, Kirschen M, Madsen JR (1999) Human theta oscillations exhibit task dependence during virtual maze navigation. *Nature* 399:781–784.
6. O'Keefe J, Recce ML (1993) Phase relationship between hippocampal place units and the EEG theta rhythm. *Hippocampus* 3:317–330.
7. Hasselmo ME, Bodelon C, Wyble BP (2002) A proposed function for hippocampal theta rhythm: Separate phases of encoding and retrieval enhance reversal of prior learning. *Neural Comput* 14:793–817.
8. Louie K, Wilson MA (2001) Temporally structured replay of awake hippocampal ensemble activity during rapid eye movement sleep. *Neuron* 29:145–156.
9. Lakatos P, *et al.* (2005) An oscillatory hierarchy controlling neuronal excitability and stimulus processing in the auditory cortex. *J Neurophysiol* 94:1904–1911.
10. Canolty RT, *et al.* (2006) High gamma power is phase-locked to theta oscillations in human neocortex. *Science* 313:1626–1628.
11. Dickson CT, Magistretti J, Shalinsky M, Hamam B, Alonso A (2000) Oscillatory activity in entorhinal neurons and circuits. Mechanisms and function. *Ann NY Acad Sci* 911:127–150.
12. Magill PJ, Sharott A, Bolam JP, Brown P (2006) Delayed synchronization of activity in cortex and subthalamic nucleus following cortical stimulation in the rat. *J Physiol* 574:929–946.
13. Pare D, Collins DR, Pelletier JG (2002) Amygdala oscillations and the consolidation of emotional memories. *Trends Cognit Sci* 6:306–314.
14. DeCoteau WE, *et al.* (2007) Learning-related coordination of striatal and hippocampal theta rhythms during acquisition of a procedural maze task. *Proc Natl Acad Sci USA* 104:5644–5649.
15. DeCoteau WE, *et al.* (2007) Oscillations of local field potentials in the rat dorsal striatum during spontaneous and instructed behaviors. *J Neurophysiol* 97:3800–3805.
16. Berke JD, Okatan M, Skurski J, Eichenbaum HB (2004) Oscillatory entrainment of striatal neurons in freely moving rats. *Neuron* 43:883–896.
17. Boraud T, Brown P, Goldberg JA, Graybiel AM, Magill PJ (2005) Oscillations in the basal ganglia: The good, the bad, and the unexpected. *The Basal Ganglia VIII*, eds Bolam JP, Ingham CA, Magill PJ (Springer Science and Business Media, New York), pp 3–24.
18. Singer W, Gray CM (1995) Visual feature integration and the temporal correlation hypothesis. *Annu Rev Neurosci* 18:555–586.
19. Fries P, Reynolds JH, Rorie AE, Desimone R (2001) Modulation of oscillatory neuronal synchronization by selective visual attention. *Science* 291:1560–1563.
20. Borgers C, Epstein S, Kopell NJ (2005) Background gamma rhythmicity and attention in cortical local circuits: A computational study. *Proc Natl Acad Sci USA* 102:7002–7007.
21. Jensen O, Kaiser J, Lachaux JP (2007) Human gamma-frequency oscillations associated with attention and memory. *Trends Neurosci* 30:317–324.
22. Harris KD, Csicsvari J, Hirase H, Dragoi G, Buzsaki G (2003) Organization of cell assemblies in the hippocampus. *Nature* 424:552–556.
23. Montgomery SM, Buzsaki G (2007) Gamma oscillations dynamically couple hippocampal CA3 and CA1 regions during memory task performance. *Proc Natl Acad Sci USA* 104:14495–14500.
24. Driver JE, *et al.* (2007) Impairment of hippocampal gamma-frequency oscillations in vitro in mice overexpressing human amyloid precursor protein (APP). *Eur J Neurosci* 26:1280–1288.
25. Lisman J (2005) The theta/gamma discrete phase code occurring during the hippocampal phase precession may be a more general brain coding scheme. *Hippocampus* 15:913–922.
26. Crone NE, Boatman D, Gordon B, Hao L (2001) Induced electrocorticographic gamma activity during auditory perception. Brazier Award-winning article, 2001. *Clin Neurophysiol* 112:565–582.
27. Edwards E, Soltani M, Deouell LY, Berger MS, Knight RT (2005) High gamma activity in response to deviant auditory stimuli recorded directly from human cortex. *J Neurophysiol* 94:4269–4280.
28. Ray S, Niebur E, Hsiao SS, Sinai A, Crone NE (2008) High-frequency gamma activity (80–150Hz) is increased in human cortex during selective attention. *Clin Neurophysiol* 119:116–133.
29. Buzsaki G, Horvath Z, Urioste R, Hetke J, Wise K (1992) High-frequency network oscillation in the hippocampus. *Science* 256:1025–1027.
30. Jensen O, Colgin LL (2007) Cross-frequency coupling between neuronal oscillations. *Trends Cognit Sci* 11:267–269.
31. Chrobak JJ, Lorincz A, Buzsaki G (2000) Physiological patterns in the hippocampo-entorhinal cortex system. *Hippocampus* 10:457–465.
32. Masimore B, Schmitzer-Torbert NC, Kakalios J, Redish AD (2005) Transient striatal gamma local field potentials signal movement initiation in rats. *NeuroReport* 16:2021–2024.
33. Brown P, *et al.* (2002) Oscillatory local field potentials recorded from the subthalamic nucleus of the alert rat. *Exp Neurol* 177:581–585.
34. Bevan MD, Magill PJ, Terman D, Bolam JP, Wilson CJ (2002) Move to the rhythm: Oscillations in the subthalamic nucleus–external globus pallidus network. *Trends Neurosci* 25:525–531.
35. Magill PJ, Sharott A, Bolam JP, Brown P (2004) Brain state-dependency of coherent oscillatory activity in the cerebral cortex and basal ganglia of the rat. *J Neurophysiol* 92:2122–2136.
36. Calabresi P, Picconi B, Tozzi A, Di Filippo M (2007) Dopamine-mediated regulation of corticostriatal synaptic plasticity. *Trends Neurosci* 30:211–219.
37. Dejean C, Gross CE, Bioulac B, Boraud T (2008) Dynamic changes in the cortex–basal ganglia network after dopamine depletion in the rat. *J Neurophysiol* 100:385–396.
38. Cohen MX, *et al.* (2008) Good vibrations: Cross-frequency coupling in the human nucleus accumbens during reward processing. *J Cognit Neurosci*, in press.
39. Kay LM (2003) Two species of gamma oscillations in the olfactory bulb: Dependence on behavioral state and synaptic interactions. *J Integr Neurosci* 2:31–44.
40. Whittington MA, Traub RD, Kopell N, Ermentrout B, Buhl EH (2000) Inhibition-based rhythms: Experimental and mathematical observations on network dynamics. *Int J Psychophysiol* 38:315–336.
41. Traub RD, *et al.* (2002) Axonal gap junctions between principal neurons: A novel source of network oscillations, and perhaps epileptogenesis. *Rev Neurosci* 13:1–30.
42. Traub RD, *et al.* (2003) GABA-enhanced collective behavior in neuronal axons underlies persistent gamma-frequency oscillations. *Proc Natl Acad Sci USA* 100:11047–11052.
43. Cunningham MO, *et al.* (2004) Coexistence of gamma and high-frequency oscillations in rat medial entorhinal cortex in vitro. *J Physiol* 559:347–353.
44. DeCoteau WE, Kesner RP (2000) A double dissociation between the rat hippocampus and medial caudoputamen in processing two forms of knowledge. *Behav Neurosci* 114:1096–1108.
45. White NM, McDonald RJ (2002) Multiple parallel memory systems in the brain of the rat. *Neurobiol Learn Mem* 77:125–184.
46. Packard MG, McGaugh JL (1996) Inactivation of hippocampus or caudate nucleus with lidocaine differentially affects expression of place and response learning. *Neurobiol Learn Mem* 65:65–72.
47. Foerde K, Knowlton BJ, Poldrack RA (2006) Modulation of competing memory systems by distraction. *Proc Natl Acad Sci USA* 103:11778–11783.
48. Mormann F, *et al.* (2005) Phase/amplitude reset and theta-gamma interaction in the human medial temporal lobe during a continuous word recognition memory task. *Hippocampus* 15:890–900.
49. Barnes T, Kubota Y, Hu D, Jin DZ, Graybiel AM (2005) Activity of striatal neurons reflects dynamic encoding and recoding of procedural memories. *Nature* 437:1158–1161.
50. Jones MW, Wilson MA (2005) Phase precession of medial prefrontal cortical activity relative to the hippocampal theta rhythm. *Hippocampus* 15:867–873.

Supporting Information

Tort *et al.* 10.1073/pnas.0810524105

SI Text

Training and Data Acquisition. Behavioral training and electrophysiology recording methods were approved by the Committee on Animal Care of Massachusetts Institute of Technology and are described in detail by DeCoteau *et al.* (1, 2). Briefly, 6 male Sprague–Dawley rats were implanted with head stages containing 12 tetrodes, with 6 tetrodes targeting the dorsomedial caudoputamen (AP: +1.7 mm, ML: 1.8 mm, DV: 3.6–4.6 mm) and 6 tetrodes targeting the CA1 region of the dorsal hippocampus (AP: −3.3 mm, ML: 2.2 mm, DV: 2.4–2.8 mm). Tetrodes were lowered to their target depths during a 1-week postsurgical recovery period. Rats then received daily training sessions (usually 40 trials) on an auditory tone-cued T-maze task. Rats were trained to turn right or left at the choice point of the maze as instructed by 1- and 8-kHz tone cues. A click warning cue preceded the opening of a start gate. Rats were rewarded with chocolate sprinkles if the baited goal was correctly approached. Throughout training, LFPs were amplified (gain: 1,000), filtered (1–475 Hz) and continuously sampled at 1 kHz by using a Cheetah recording system (Neuralynx). An anchor screw in the rat's skull or the external ground of the recording system was used as reference. In some sessions, a striatal tetrode was used as reference to verify local generation of striatal field potentials. Tetrode tracks and microlesions marking the final tetrode position were identified in 24-μm-thick sections of formalin-fixed tissue stained for Nissl substance. In the hippocampus, the definition of "deep" and "superficial" CA1 layers was performed based on the phase reversal of the theta wave combined with daily records of tetrode depth.

Data Analysis. All analyses were done by using MATLAB 7.5 software by MathWorks. Computations were carried out on an Intel Pentium III Linux Cluster at Boston University (http://scv.bu.edu/computation/linuxcluster/). Unless otherwise specified, the analyses were performed on 1,000-ms windows centered at the task events.

The modulation index and the phase-to-amplitude comodulograms. To quantify the amplitude modulation by phase, we created a modulation index (MI) based on a normalized entropy measure previously described in Hurtado *et al.* (3). This index is able to detect cross-frequency coupling between 2 frequency ranges of interest. We denote the amplitude and the phase frequency ranges under analysis by f_A and f_p, respectively. We denote as $x_{\text{raw}}(t)$ the raw signal (i.e., the unfiltered LFP; Fig. S2*a*). The MI is calculated as described below (see Fig. S2).

1. First, $x_{\text{raw}}(t)$ is filtered at the 2 frequency ranges under analysis (f_p and f_A). We denote the filtered signals as $x_{fp}(t)$ and $x_{fA}(t)$ (Fig. S2 *b* and *c*).
2. The time series of the phases of $x_{fp}(t)$ [denoted as $\phi_{fp}(t)$] is obtained from the standard Hilbert transform of $x_{fp}(t)$ (Fig. S2*d*). The Hilbert transform is also applied to $x_{fA}(t)$ to extract the time series of the amplitude envelope of $x_{fA}(t)$ [denoted as $A_{fA}(t)$; (Fig. S2*e*)]. The composite time series $[\phi_{fp}(t),A_{fA}(t)]$ is then constructed, which informs the amplitude of the f_A oscillation at each phase of the f_p rhythm (Fig. S2*f*).
3. Next, the phases $\phi_{fp}(t)$ are binned into eighteen 20° intervals (0° to 360°), and the mean of A_{fA} over each phase bin is calculated (Fig. S2*g*). We denote as $\langle A_{fA}\rangle_{\phi_{fp}}(j)$ the mean A_{fA} value at the phase bin j.
4. We then apply the entropy measure H, defined by:

$$H = -\sum_{j=1}^{N} p_j \log p_j,$$

where $N = 18$ (i.e., the number of bins) and p_j is given by

$$p_j = \frac{< A_{f_A} >_{\phi_{f_p}}(j)}{\sum_{j=1}^{N} < A_{f_A} >_{\phi_{f_p}}(j)}.$$

5. The MI is finally obtained by normalizing H by the maximum possible entropy value ($H_{\max}$), which is obtained for the uniform distribution $p_j = 1/N$ (and hence $H_{\max} = \log N$):

$$MI = \frac{H_{\max} - H}{H_{\max}}.$$

A MI value of 0 indicates lack of phase-to-amplitude modulation (i.e., constant $\langle A_{fA}\rangle_{\phi_{fp}}$ for all phase bins), and larger MI values result from stronger phase-to-amplitude modulation.

The comodulogram plot is obtained by representing in pseudocolor scale the MI values of multiple (f_p,f_A) pairs, with f_p calculated in 1-Hz steps with 2-Hz bandwidths and f_A in 2-Hz steps with 4-Hz bandwidths (Fig. S2*i*). We note however that the comodulogram plots reported in the figures of the main article were further subjected to statistical analysis (described below), and the value of each (f_p,f_A) entry was obtained by $MI_{\text{stat}} = MI - MI_{\text{thresh}}$, where MI_{thresh} is the significance threshold. Any value >0 in the comodulogram plots shown in the main article is statistically significant.

The MI statistical analysis. To assess the statistical significance of the MI values, we worked with a distribution of 200 surrogate MI values achieved by applying the MI measure to trial shuffled composite time series $[\phi_{fp}(t),A_{fA}(t)]$. To create the trial shuffled composite time series, $\phi_{fp}(t)$ is calculated from trial m, and $A_{fA}(t)$ is calculated from trial n, with m and n randomly chosen from $[1.,K]$, K denoting the total number of trials (usually $K = 40$ in each session). Assuming a normal distribution of the surrogate MI values, a significance threshold (MI_{thresh}) is then calculated by using $P < 0.01$.

Remark: Canolty *et al.* (4) used a modulation index that is computed based on the mean vector of a complex time series defined by $A_{fA}(t)e^{i\phi_{fp}(t)}$ compared with a distribution of surrogate means created by offsetting $A_{fA}(t)$ and $\phi_{fp}(t)$ by some large time lag τ (i.e., a surrogate vector is defined by $A_{fA}(t + \tau)e^{i\phi_{fp}(t)}$; see supporting information of ref. 4). We worked with the modulation index described above instead of their measure because large time records are required to create the surrogate data necessary to compute the Canolty *et al.* index; we did not have such long records (each trial lasts a few seconds, and the task events were analyzed in 1,000-ms windows). Nevertheless, we observed the same qualitative results when working with a variant of Canolty *et al.* index, which was obtained by using the shuffled trial procedure to create the surrogate data (data not shown). However, we again chose to work with our modulation index instead of this variant because our index is potentially able to detect bimodal distributions of phase of maximal amplitude that would not be seen by the mean vector analysis (e.g., if the gamma amplitude of a given signal is modulated by the theta

phases of ϕ and of $\phi + \pi$, then the amplitude peaks would cancel the other in the mean vector analysis).

Theta trough time-locked plots. The time–frequency plots of the mean normalized power time-locked to the theta trough were computed as described in Canolty *et al.* (4). Briefly, the theta troughs are identified by finding the local minima of the phase time series (obtained by applying the Hilbert transform to the theta-filtered signal). A set of normalized instantaneous power series is calculated as follows: first the raw signal $x_{raw}(t)$ is filtered into several bands with center frequencies from 10 to 400 Hz, in 2-Hz steps with 4-Hz bandwidths; next, each band-pass-filtered signal is normalized by subtracting the temporal mean and dividing by the temporal standard deviation; last, the amplitude envelope is calculated for each normalized signal (by using the Hilbert transform) and subsequently squared element-wise. The time–frequency plot is generated by averaging 800-ms epochs extracted from the normalized instantaneous power centered at the theta troughs (producing what was defined as the mean normalized power time-locked to the theta trough). The theta trough time-locked plots were computed by using LFP data between the "Start" and "Turn-End" task events.

Averaged raw signals centered at the fast oscillations peaks. The results shown in Figs. 3*B* and 4 *B* and *C* and Fig. S4*b* were obtained as follows: first the signal was filtered at the fast oscillation frequency range under study (e.g., 80–120 Hz, HG or HFO). Then, a time series indicating the times of the peaks of the filtered signal was constructed, with the requirement that the peak times are separated by at least 100 ms from each other (i.e., just the highest peaks within 100-ms windows were used; the requirement of 100 ms is to avoid selecting multiple peaks within a theta cycle). The final trace is then obtained by averaging 600-ms epochs of the raw signal centered at the time points corresponding to the fast oscillation peaks. Note that if the fast oscillation peaks occur more often in a given theta phase (e.g., at the trough of the oscillation), one expects to be able to observe both the fast oscillation and the theta wave in the averaged raw signal, because the theta waves are time-locked to the peak times. On the other hand, if the fast oscillation possesses no amplitude modulation by the theta phase, the theta waves will be out of phase among the several epochs and will be averaged out from the final mean LFP trace. In applying this measure, no assumptions regarding the phase frequency of the cross-frequency coupling are made; just the frequency band under study for amplitude modulation is required as input data. However, by also filtering the signal at the theta band and extracting the time series of the theta phases, one can assess the phases where the fast oscillation peaks occurred. A histogram showing the number of peaks in each theta phase can then be constructed and used as another tool to assess phase-to-amplitude coupling. Such histograms are reported together with the averaged LFP traces in the figures. The averaged raw signals centered at the fast oscillation peaks and the corresponding histograms were computed by using LFP data between the Start and Turn-End task events.

Multiple regression analyses. Multiple regression analysis was performed by using MATLAB *regress.m* function. The regression analysis was used to study relations between the cross-frequency couplings and the power of the rhythms. More specifically, we studied the relations between power and the MI values obtained for the fast oscillations amplitude and the theta phase. In Figs. S6–S9, the intensity of the cross-frequency coupling, or "modulation," was assessed by the $\langle MI \rangle_\theta$ value. The symbol $\langle MI \rangle_\theta$ denotes the mean MI values calculated over a rectangular area of the comodulogram plot defined by the intersection of theta range (in the phase axis) and the fast oscillation range under study (in the amplitude axis). For example, HFO $\langle MI \rangle_\theta$ is obtained by calculating the mean over the (f_p, f_A) entries pertaining to the rectangle (7, 12)Hz × (120, 180)Hz. Similarly, LG $\langle MI \rangle_\theta$ is calculated over (7, 12)Hz × (30, 60)Hz, and HG $\langle MI \rangle_\theta$ is the mean over (7, 12)Hz × (60, 100)Hz. Lastly, 80–120 Hz $\langle MI \rangle_\theta$ denotes the *MI* mean over (5, 9)Hz × (80, 120)Hz as the amplitude modulation occurred in a lower theta range in the striatum. We note that we chose to work with the mean over the comodulogram entries ($\langle MI \rangle_\theta$) as opposed to computing the MI for wide-band-filtered signals because the latter analysis may be affected by the 1/*f* power distribution. For example, take the case in which the amplitude of 85–95 Hz is modulated by the theta phase. This narrow band modulation might not be evident when one calculates the MI for the signal wide-band filtered at the HG range (60–100 Hz). This is because the amplitude envelope of the HG-filtered signal is mainly due to the frequencies near 60 Hz (by 1/*f*, the lower the frequency, the higher the amplitude), which present no modulation by the theta phase in this example.

The mean modulation index values ($\langle MI \rangle_\theta$) were subjected to regression analyses against the power of the distinct rhythms. Before this procedure, however, the $\langle MI \rangle_\theta$ value in each task event was expressed as the ratio to the pre-trial value, and the power values were expressed as *z*-scores. This normalization was performed to allow the combined analysis of distinct electrodes and animals.

Cross-structure cross-frequency coupling analysis. The comodulograms generated during the cross-structure coupling analysis were obtained by following the same steps as described above for the analysis within each structure. However, the phase time series ϕ_{fp} and the amplitude time series A_{fA} were each obtained from a different region, as labeled in Fig. 5*A*. We note that there are 2 ways in which the phase of a low-frequency oscillation in structure *X* (defined as X_f) could modulate the amplitude of a high-frequency oscillation in structure *Y* (defined as Y_{fA}). The first consists of cross-frequency coupling within structure *Y* (i.e., $Y_{fp} \rightarrow Y_{fA}$) combined with high phase coherence at low frequencies between *Y* and *X*. The result is an indirect coupling between structures: $X_{fp} \rightsquigarrow Y_{fA}$; because the (low frequency) phase in *Y* and (low frequency) phase in *X* are strongly coherent, the phase in *X* appears to modulate the (high frequency) amplitude of *Y*. The second consists of direct cross-frequency coupling between structures: $X_{fp} \rightarrow Y_{fA}$. In this case, the (low frequency) phase of *X* modulates the (high frequency) amplitude of *Y*, irrespective of the (low frequency) phase coherence levels between *X* and *Y*. The presence of strong phase coherence between *X* and *Y*, as observed in this study between the hippocampus and the striatum, does not by itself invalidate the possibility of a direct interaction between X_{fp} and Y_{fA}.

Speed-controlled analyses. The same animal was used in Fig. S8 *A–C*, and the means were taken over several experimental sessions ($n = 13$). The group results (over rats, electrodes, and experimental sessions) shown in Fig. S8*D* were obtained during the Tone Onset event. Within each experimental session, the trials were divided into 4 groups according to the rat's speed [i.e., divided into 4 speed quartiles (IQ)]. The mean MI values ($\langle MI \rangle_\theta$, see session above) were then computed for each IQ group. The LG, HG, and HFO $\langle MI \rangle_\theta$ values were computed over the hippocampal electrodes, and the 80- to 120-Hz $\langle MI \rangle_\theta$ over the striatal electrodes. Each IQ group within an experimental session included ≈10 trials (i.e., sessions typically consisted of 40 trials). To allow the combined analyses of distinct animals, electrodes, and sessions, the $\langle MI \rangle_\theta$ values were normalized by dividing each IQ $\langle MI \rangle_\theta$ value by the mean over the quartiles.

Filter settings. All filtering used for the data analysis was done by using a linear finite impulse response (FIR) filter by means of *eegfilt()* function from the EEGLAB toolbox (5), which is available for free download at http://sccn.ucsd.edu/eeglab/. The filter order depends on the low-frequency cutoff, and it is given by 3 times the ratio of the sampling frequency to the low-frequency cutoff (rounded to the nearest integer toward zero). The *eegfilt()* function calls the Matlab routine *filtfilt()*, which applies the filter forward and then again backward, to ensure that

phase delays introduced by the filter are nullified. Nevertheless, we note that the absolute phase in our and other studies should be interpreted with caution, because recent evidence has been suggesting the existence of phase distortions secondary to particular characteristics of electrodes (6).

As mentioned in *Training and Data Acquisition*, above, all of the LFP data analyzed in Matlab had been previously band-pass filtered between 1 and 475 Hz by using the Cheetah recording system. We note that this procedure could be causing an artificial 3-Hz peak seen in the striatal power spectra during the first task events (Fig. 1*C*), which would otherwise look like a typical 1/*f* curve. This band-pass filtering, however, does not influence the spectral peaks at higher theta frequencies seen in the striatum during the middle of the task (e.g., during the Tone Onset event). We also observe that the maximum active frequency in the HFO band detected in our study could be influenced by low-pass filtering at 475 Hz. However, we do not believe this is a major concern because (*i*) several of our comodulograms showed modulated HFO with a limited frequency range, which were considerably below 475 Hz, and (*ii*) our analyses (more specifically, the comodulograms and the time–frequency plots locked to the theta trough) are normalized to the power of the oscillation; it is known that, whereas filtering considerable attenuates the amplitude of an oscillation, it does not completely remove it from the signal.

Remark: We were unable to analyze the relationship between the spikes and the LFPs recorded on the tetrodes due to incomplete spike datasets for enough tetrodes for sufficient numbers of simultaneous recordings. Such studies will be critical for understanding how the activities of single neurons and of neural ensembles are related to the cross-frequency couplings described here.

1. DeCoteau WE, *et al.* (2007) Learning-related coordination of striatal and hippocampal theta rhythms during acquisition of a procedural maze task. *Proc Natl Acad Sci USA* 104:5644–5649.
2. DeCoteau WE, *et al.* (2007) Oscillations of local field potentials in the rat dorsal striatum during spontaneous and instructed behaviors. *J Neurophysiol* 97:3800–3805.
3. Hurtado JM, Rubchinsky LL, Sigvardt KA (2004) Statistical method for detection of phase-locking episodes in neural oscillations. *J Neurophysiol* 91:1883–1898.
4. Canolty RT, *et al.* (2006) High gamma power is phase-locked to theta oscillations in human neocortex. *Science* 313:1626–1628.
5. Delorme A, Makeig S (2004) EEGLAB: An open source toolbox for analysis of single-trial EEG dynamics including independent component analysis. *J Neurosci Methods* 134:9–21.
6. Nelson MJ, Pouget P, Nilsen EA, Patten CD, Schall JD (2008) Review of signal distortion through metal microelectrode recording circuits and filters. *J Neurosci Methods* 169:141–157.

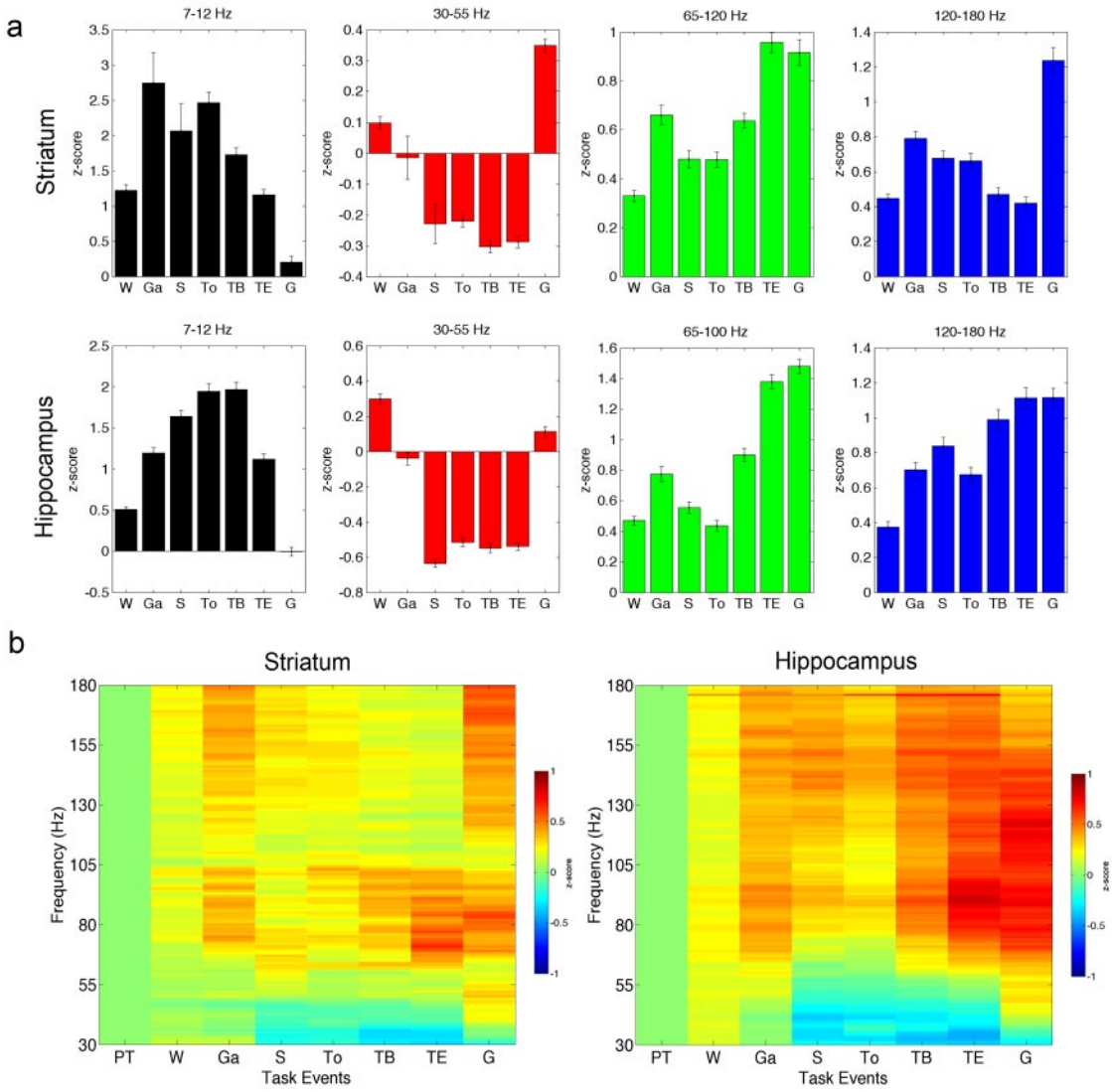

Fig. S1. Distinct frequency bands exhibit different power variations during the T-maze task. (*a*) Changes in the striatal (*Upper*) and hippocampal (*Lower*) oscillations power during distinct task events. Results are reported as the *z*-score of the average power with respect to the pre-trial average power in each frequency band. We show the average over all tetrodes, sessions, and animals (striat $n = 303$; hipp $n = 360$). Similar power variations were found in both the striatum and in the hippocampus: theta power (black bars) increases during the task, peaking at the middle of the maze, and decays to pre-trial values when the goal is approached. Low gamma power (LG, red bars) diminishes during the middle of the task, whereas high gamma (HG, green bars) and high-frequency oscillations (HFO, blue bars) powers tend to increase throughout the task events (notice, however, the difference in definition of high gamma in the striatum, in accordance with the results presented in Figs. 1 and 3 in the main article). Qualitatively similar results were found when each rat was analyzed individually. Error bars represent SEM. (*b*) Event-frequency power decomposition of striatal (*Left*) and hippocampal (*Right*) LFPs. Pseudocolor scale represents *z*-score with respect to the pre-trial period averaged over all tetrodes, sessions, and animals. Note that although the HG and HFO bands seem to be indistinguishable in the hippocampus, other analyses performed in this work revealed that they are distinct physiological processes. Events labels: PT, pre-trial; W, warning; Ga, gate; S, start; To, tone onset; TB, turn begin; TE, turn end; G, goal.

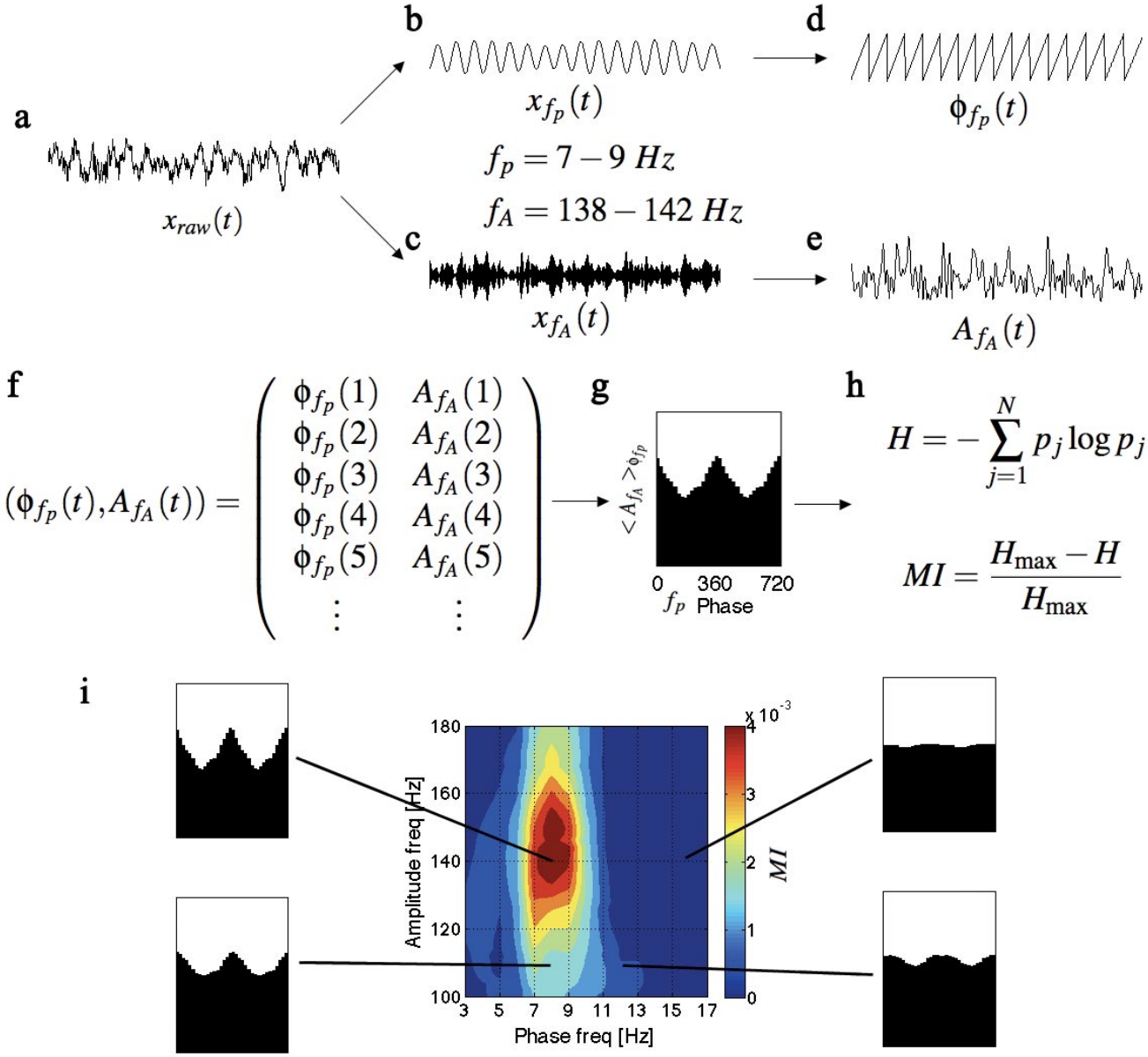

Fig. S2. Steps in the computation of the modulation index (MI) and of the comodulogram plot (see *Data Analysis* in SI Text). (*a*–*c*) The raw signal (*a*) is filtered at the phase (*b*) and amplitude (*c*) frequency ranges of interest. (*d* and *e*) Next, the phase (*d*) and the amplitude (*e*) time series are calculated from the filtered signals by using the Hilbert transform. (*f* and *g*) A composite time series (*f*) is then constructed and used to obtain the mean amplitude values at each 20° phase bin (*g*) (2 cycles shown for clarity). (*h*) The MI is finally obtained by applying a normalized entropy measure to the mean amplitude vector. (*i*) The comodulogram plot is constructed by representing in pseudocolor scale the MI values of multiple phase–amplitude frequency pairs.

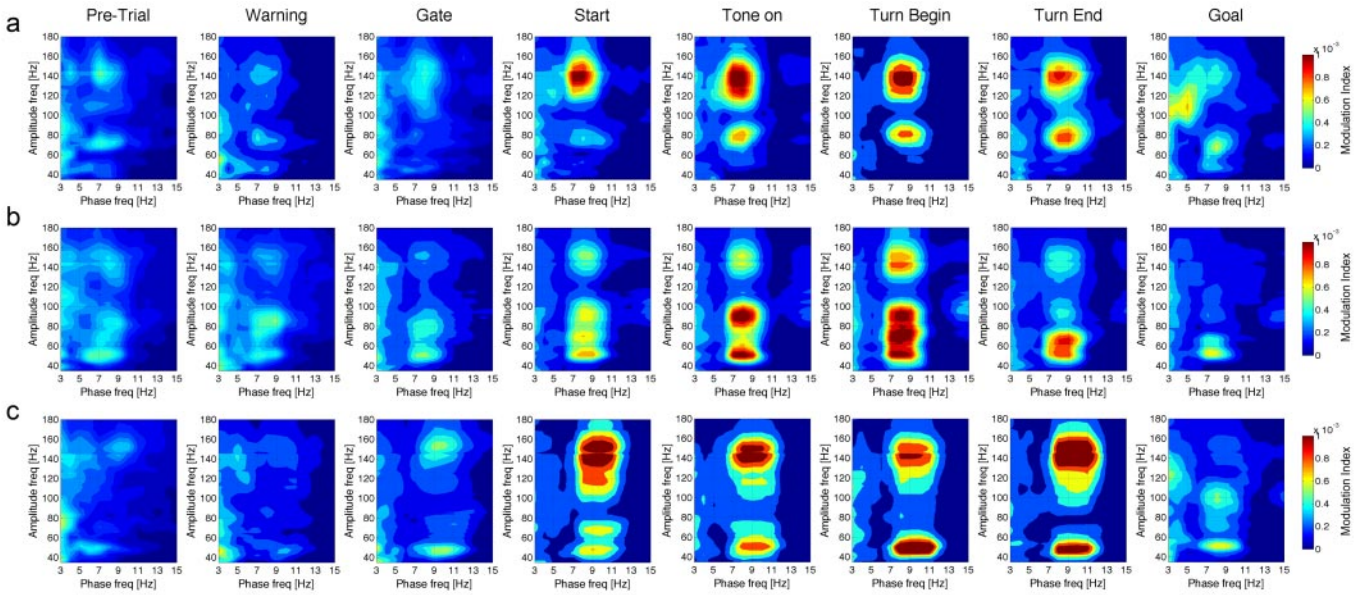

Fig. S3. Cross-frequency couplings can occur at LG, HG, or in the whole gamma range simultaneously. Rows (*a*–*c*) show the phase-to-amplitude comodulograms (obtained at the distinct task events) of 3 additional rats. In *a*, theta phase amplitude modulation occurred more in the HG band than in the LG band; in *b*, the entire gamma band was modulated by the theta phase; and in *c*, modulation appeared more in the LG band. Notice further that *b* constitutes an example of a tetrode that presented much higher modulation at the gamma range than at the HFO range. For each rat, the results were obtained from 1 representative tetrode located at the superficial layers of the dorsal CA1 region averaged over sessions (*a* and *c*: 5 sessions; *b*: 10 sessions).

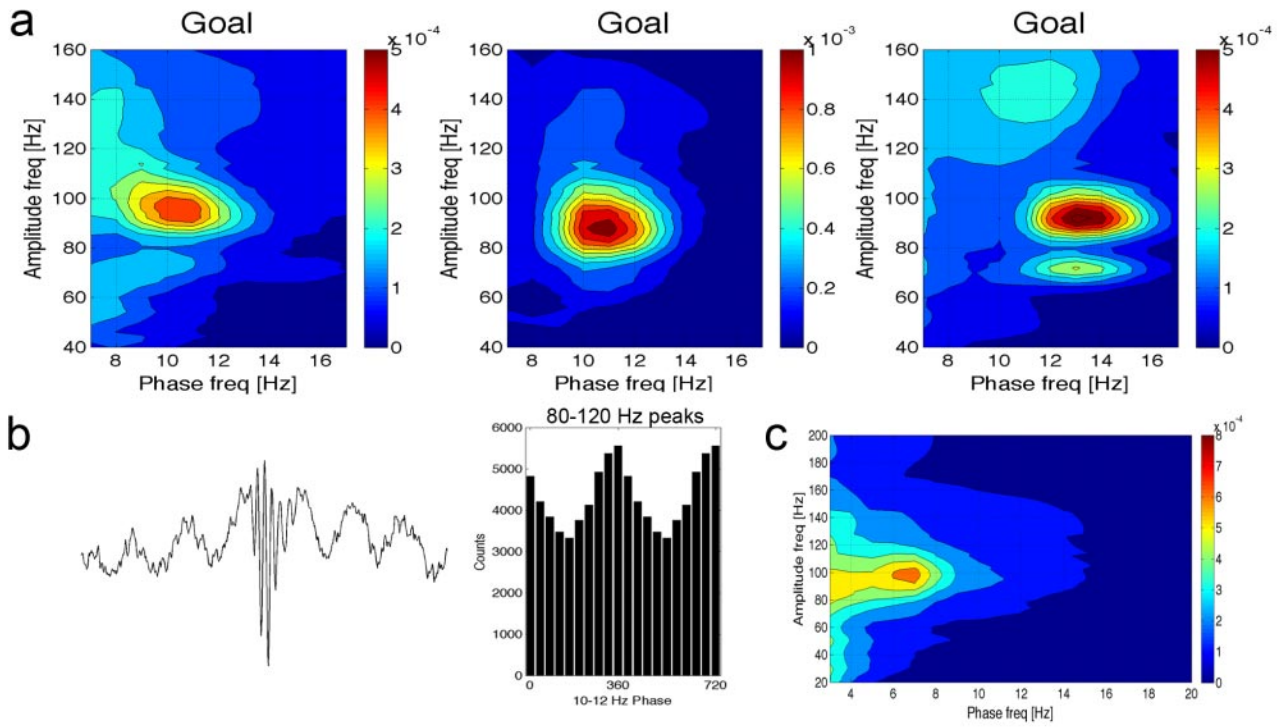

Fig. S4. The amplitude of the 80- to 120-Hz band is modulated by a ''high'' theta oscillation in the striatum during the task goal. (*a*) Phase-to-amplitude comodulograms of 3 distinct animals. These 3 rats presented an amplitude modulation of the 80- to 120-Hz frequency band by a high theta frequency during the goal period. Note, however, that their peak phase modulation frequency differed. (*b*) Averaged raw signal (600 ms shown) during the goal event obtained by centering the signal at the peaks of the 80- to 120-Hz oscillation (*Left*; see *SI Text*) and the phase histogram of the 80- to 120-Hz oscillation peaks (*Right*). Note that the high theta oscillation can be seen in the averaged raw data and that the 80- to 120-Hz oscillation peaks at the trough of this oscillation. (*c*) Phase-to-amplitude comodulogram averaged over all task events. Because the modulation by the high theta occurred only during the final period of the task, this effect cannot be noticeable in this procedure. Note further that the 80- to 120-Hz amplitude modulation by the ''low'' theta oscillation is prominent in such analysis. *a* was obtained by averaging the results of all striatal tetrodes and sessions (for each rat); *b* was obtained by averaging all striatal tetrodes during 1 session of the animal shown at the middle of *a*; *c* was obtained by averaging the results of all 3 animals.

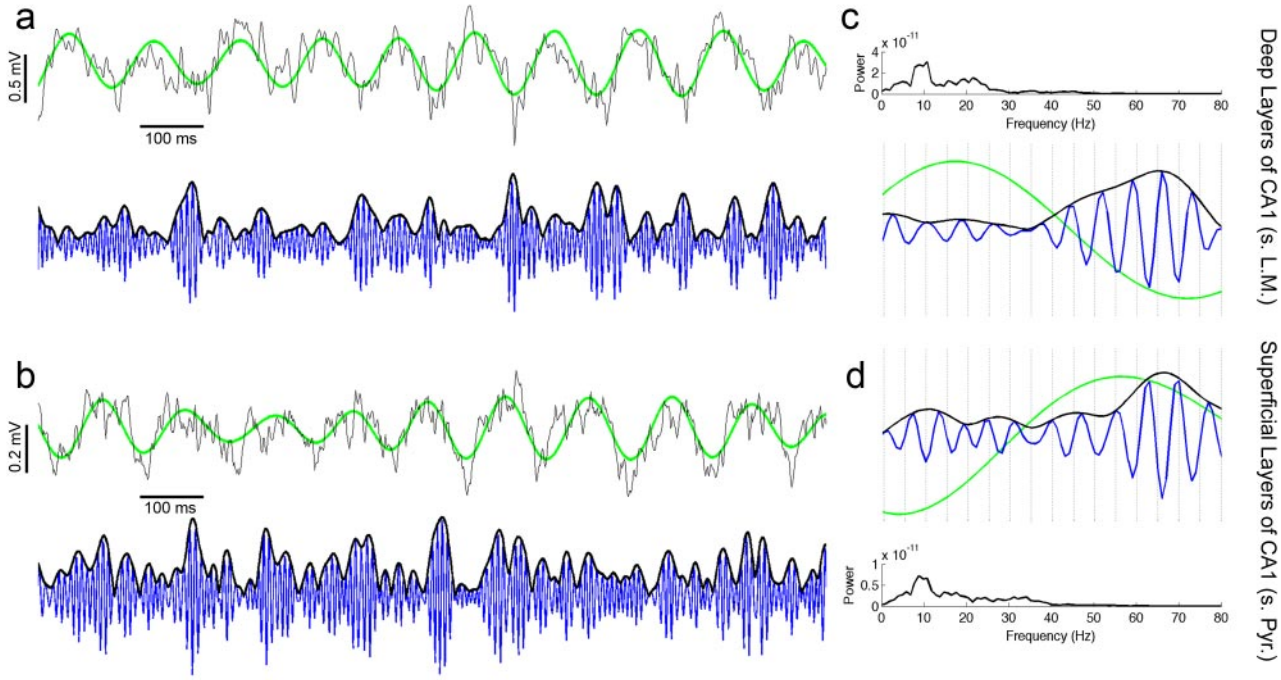

Fig. S5. The theta phase of peak HFO amplitude reverses between superficial and deep CA1 layers. (*a*) Representative hippocampal LFP trace and filtered signals during a single trial. Raw trace (thin black line) and the theta (7–12 Hz) filtered signal (thick green line) obtained from 1 tetrode located at the deep layers of the CA1 region are shown at the top (1 s shown). The (amplified) HFO (120–160 Hz) filtered signal is shown at the bottom (thin blue line). The thick black line represents the HFO amplitude envelope. (*b*) Same as in *a* but for a tetrode located at the superficial layers of the CA1 recorded simultaneously. (*c* and *d*) Power spectrum (in V^2/Hz) of the HFO amplitude envelope and an expanded view of the filtered signals [100 ms shown (corresponding to the horizontal bars in *a* and *b*)]. Note the phase reversal of both theta (green) and HFO (blue) signals between the superficial and deep CA1 layers. Notice further that the theta peak in the amplitude envelope power spectrum constitutes yet another independent analysis demonstrating the modulation of HFO by the theta rhythm.

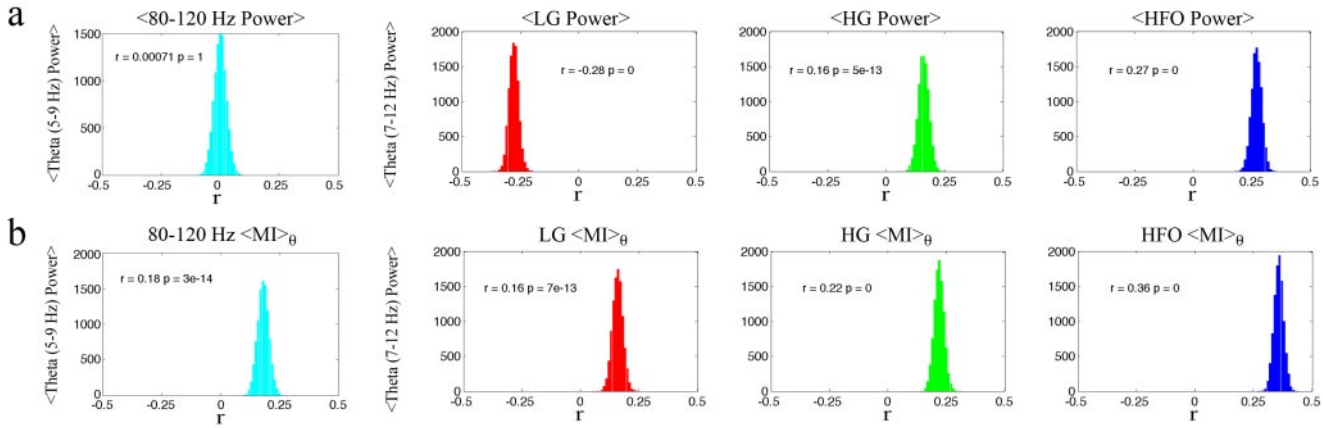

Fig. S6. Theta power correlates with the power of fast oscillations and cross-frequency coupling strength. (*a*) Bootstrap analysis (10,000 replicates) applied to the correlation coefficient (*r*) between theta power and the power of the fast oscillations. Theta power is not correlated with the 80- to 120-Hz oscillation power in the striatum (cyan). In the hippocampus, theta power is negatively correlated with LG power (red), whereas it is positively correlated with both HG (green) and HFO (blue) powers. (*b*) Bootstrap analyses of the correlation coefficient between theta power and the averaged modulation index ($\langle MI \rangle_\theta$) values of striatal and hippocampal fast oscillations, showing that theta power is positively correlated with the intensity of phase-to-amplitude modulation of all higher-frequency rhythms studied. Results were obtained from the pooled data of all tetrodes, sessions, and animals (striatum: $n = 303$; hippocampus: $n = 360$). Both the mean power values and $\langle MI \rangle_\theta$ were normalized to permit combined analyses of distinct tetrodes and animals (see *SI Text*).

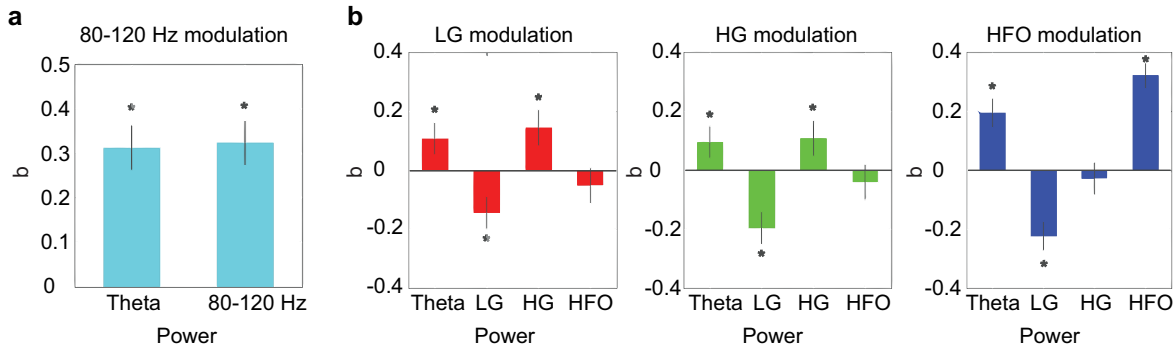

Fig. S7. Cross-frequency couplings depend on the power of multiple frequency bands. Plots show standardized regression coefficients obtained from multiple regression analyses between the intensity of the amplitude to theta phase modulation (dependent variable) and the mean power of frequency bands of interest (independent variables). (*a*) Regression analysis of striatal LFP recordings, showing that the modulation of 80- to 120-Hz oscillations depend equally on their own power and on the power of cooccurring theta rhythms. (*b*) Regression analysis for 3 high-frequency oscillations in the hippocampus. Notice that the theta modulation of HG and HFO are mutually independent. These results were obtained from the pooled data of all tetrodes, sessions, and animals (striatum: $n = 303$; hippocampus: $n = 360$). The vertical black lines represent the 99% confidence intervals. *, statistically significant coefficients ($P < 0.00001$). The intensity of theta phase modulation was assessed by computing the mean modulation index values at the theta band (see *SI Text*).

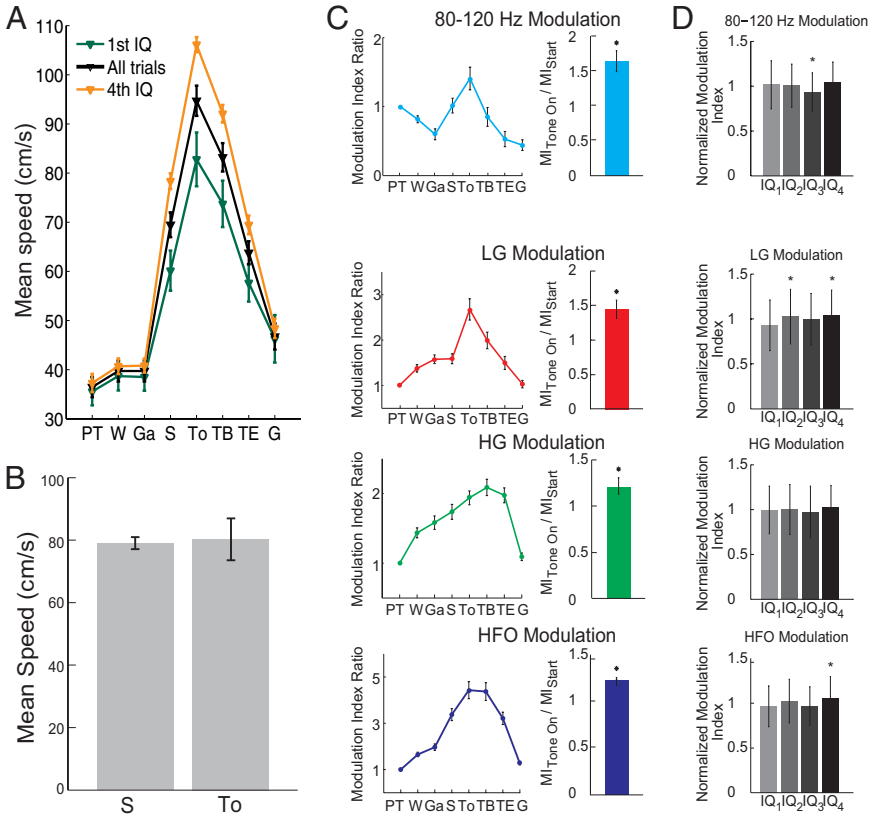

Fig. S8. Running speed does not account for the different intensities of cross-frequency phase-amplitude couplings during different task epochs. (*A*) Mean speed as a function of the task event for the animal shown in Fig. 2. The black trace shows the mean speed over all trials and sessions. The orange and the green traces show the mean speed for the fastest and the slowest quartile trials, respectively. Error bars represent SEM. (*B*) Mean speeds of subset of trials for this animal chosen to equate the running speed for the ''Tone Onset'' and ''Start'' task events (i.e., the fastest trials for the Start event and the slowest trials for the Tone Onset event were chosen). These trials were used for the analysis in *C*. (*C*) (*Left*) Mean modulation index (MI) values for striatal 80–120 Hz (top row) and hippocampal high-frequency rhythms (bottom 3 rows, as labeled), expressed as a ratio of the pre-trial MI value, as a function of the task event for all trials and sessions for the same animal as in *A*. (*Right*) Mean MI ratio between the Tone Onset and Start events computed over the speed-controlled trial subsets from *B*. *, statistically significant difference from 1 ($P < 0.05$, paired *t* test). (*D*) Normalized MI versus speed computed for each speed interquartile (IQ1 to IQ4: slowest to fastest) and averaged over all rats, tetrodes, and sessions (see *SI Text*). Note the absence of meaningful differences in MI values across the quartiles; in particular, notice that the MI values are not increasing across the quartiles. Bars represent SD. *, $P < 0.05$ (Friedman test).

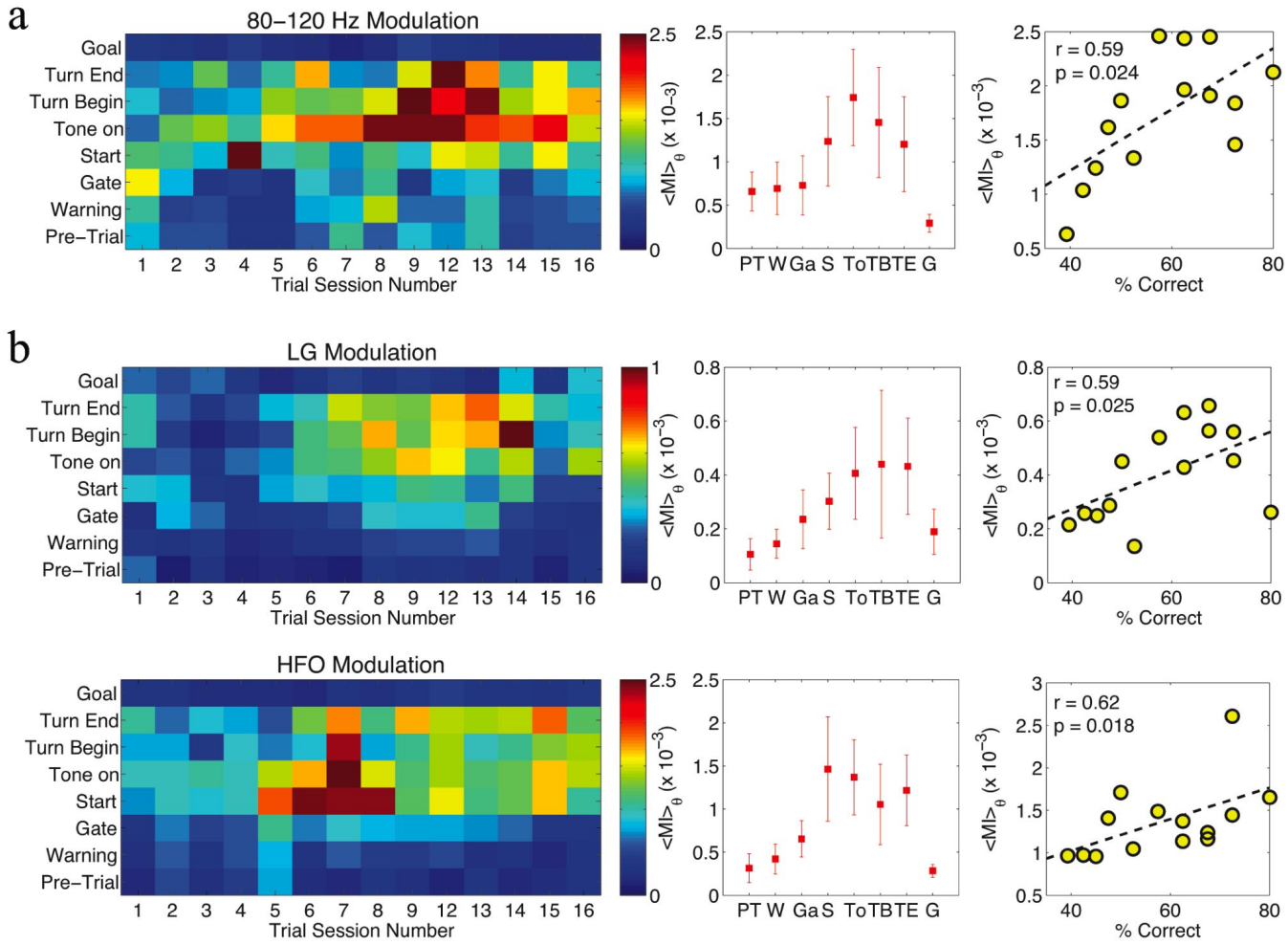

Fig. S9. Intensity of amplitude modulation may correlate with learning. (*a*) (*Left*) Pseudocolor plot showing average modulation index ($\langle MI \rangle_\theta$) values as a function of task event and session number for striatal 80–120 Hz modulated by theta. (*Center*) The mean $\langle MI \rangle_\theta$ values as a function of the trial event obtained by averaging $\langle MI \rangle_\theta$ over all sessions. Error bars represent SEM. (*Right*) Correlation between $\langle MI \rangle_\theta$ during the Tone Onset event and percent correct performance. (*b*) (*Left*) $\langle MI \rangle_\theta$ as a function of task event and session number for hippocampal LG (upper plot) and HFO (lower plot) modulated by theta. (*Center*) Mean hippocampal $\langle MI \rangle_\theta$ versus task event for LG (*Upper*) and HFO (*Lower*) averaged over all sessions. (*Right*) Correlation between $\langle MI \rangle_\theta$ and percent correct for hippocampal LG and HFO. Results in *A* and *B* were obtained from 1 tetrode in the striatum and in the superficial layers of CA1, respectively, that did not move their positions during the sessions analyzed. We could not, however, consistently study the correlation of the modulation index with learning because most of the tetrodes moved their position across the sessions (e.g., from deep to superficial CA1 layers) and also because some animals were subjected to distinct number of trials in different experimental session days. Both factors make unreliable a direct comparison of the modulation index across distinct experimental sessions (for instance, the intensity of the modulation depends on the theta power (Figs. S6 and S7) and theta power is known higher in the striatum lacunosum-moleculare (corresponding to deep layers recordings) than in striatum pyramidale (superficial layers recordings); note the change in the *y*-scale between Fig. S5 *a* and *b*).